

Modulation Doping: A Strategy for 2D Materials Electronics

Dan Wang, Xian-Bin Li,* and Hong-Bo Sun*



Cite This: <https://doi.org/10.1021/acs.nanolett.1c02192>



Read Online

ACCESS |



Metrics & More



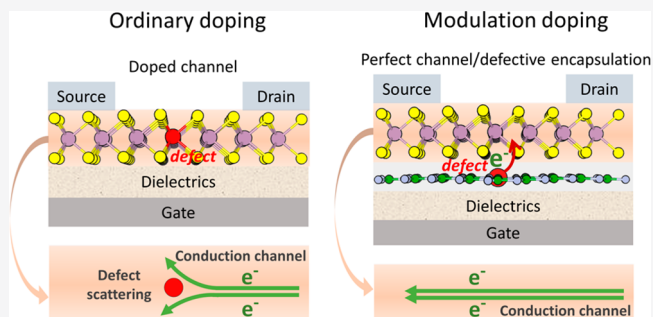
Article Recommendations



Supporting Information

ABSTRACT: It remains a remarkable challenge to develop practical techniques for controllable and nondestructive doping in two-dimensional (2D) materials for their use in electronics and optoelectronics. Here, we propose a modulation doping strategy, wherein the perfect n-/p-type channel layer is achieved by accepting/donating electrons from/to the defects inside an adjacent encapsulation layer. We demonstrate this strategy in the heterostructures of BN/graphene, BN/MoS₂, where the previously believed useless deep defects, such as the nitrogen vacancy in BN, can provide free carriers to the graphene and MoS₂. The carrier density is further modulated by engineering the surroundings of the encapsulation layer. Moreover, the defects and carriers are naturally separated in space, eliminating the effects of Coulomb impurity scattering and thus allowing high mobility in the 2D limit. This doping strategy provides a highly viable route to tune 2D channel materials without inducing any structural damage, paving the way for high-performance 2D nanoelectronic devices.

KEYWORDS: 2D materials, modulation doping, encapsulation layer, channel layer, high mobility, p-type MoS₂



INTRODUCTION

Doping of semiconductors, the way of modulating charge carriers (including type and concentration) and controlling electrical conduction, has been the key technology for the development of electronics and optoelectronics.^{1–3} Highly tunable doping levels and negligible structural damage to the materials are both desirable for realizing controllable and effective doping. The great potential of two-dimensional (2D) materials for applications in microelectronics and nanoelectronics has promoted the progress of several doping techniques, such as electrostatic doping,^{4,5} where carriers are provided by the electric field without changing the channel material chemical composition, and molecular doping,^{6,7} which relies on the charge transfer between the surface molecules and the 2D layer. However, the practical applications of such doping techniques are limited by the electrical breakdown (or sophisticated device fabrication)^{8,9} and molecular instability,^{6,10} respectively. The widely utilized doping technique in semiconductors is ion implantation. Nonetheless, it has also proved to be challenging for 2D materials because of their atomically thin nature.^{11,12} The process of bombarding the semiconductor with energetic alien atoms (or impurities) may cause serious damage or induce considerable and undesirable defects to the 2D structure.

What is worse, because of the weak screening, defects in 2D materials are predicted to be generally deep with ionization energy much larger than the thermal energy.^{2,13–17} Deep-level defects are usually not appreciated in electronics since they serve as scattering centers (decreasing carrier mobilities) or

charge recombination centers (reducing carrier lifetime), resulting in degraded performance of devices.^{18–20} This suggests even with a stable doping technique for 2D materials, defects in such materials may not be utilized to achieve satisfiable electrical conductivity. Field-effect transistors made of 2D materials, in general, suffer from retarded carrier mobility. This has been recognized as a main limiting factor by the industry like TSMC^{21,22} for harvesting the potential of 2D materials in next-generation nanoelectronics. Thus, it is highly advisable to develop a new doping strategy for 2D electronics, to maintain structural integrity while at the same time obtain high carrier density and mobility by converting deep-level defects to shallow defects.

In this paper, we propose such a doping strategy based on heterostructure engineering. Instead of introducing defects into the channel 2D material, we place the defect only in the encapsulation 2D material that forms a heterostructure with the channel material. The encapsulation layer prevents the channel layer from being impaired during the process of defect formation such as the ion implantation. Meanwhile, the defect in the encapsulation layer donates/accepts its electron to/from the channel layer, allowing modulation of conductivity in the

Received: June 4, 2021

Revised: June 28, 2021

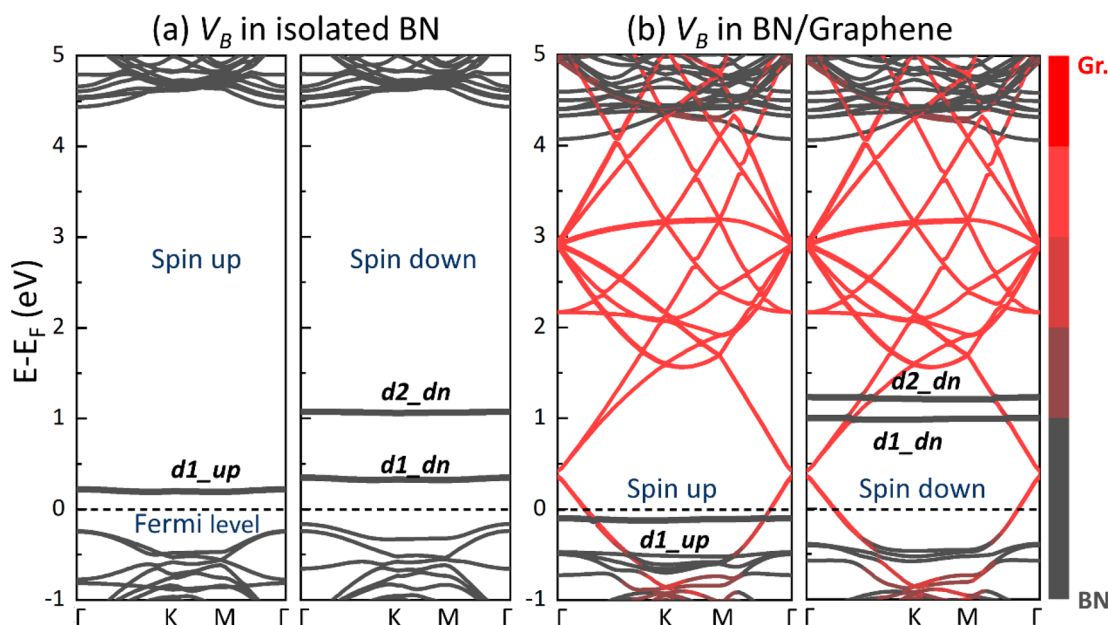


Figure 1. (a) Band structure of V_B in isolated BN. (b) Projected band structure of V_B in the heterostructure of BN/Graphene with red and black colors indicating weights of graphene and BN atomic orbital projections. The thick lines stand for the defect states induced around the Fermi level as indicated by the 0-eV line.

channel layer. Through first-principles calculations, we successfully predicted the electron/hole transfer from the deep-level nitrogen/boron vacancy in monolayer BN to monolayer graphene, demonstrating robust n-/p-type doping of the graphene. The charge transfer still holds even with the system where one more perfect BN layer is inserted between the graphene and the defective BN layer. Moreover, by adopting this strategy, we achieved a perfect n-type and p-type MoS_2 in the heterostructure of BN/ MoS_2 (the BN is with a nitrogen-vacancy) and $\text{ZrS}_2/\text{MoS}_2$ (one NO molecule adsorbed on one sulfur vacancy of ZrS_2), respectively. Our strategy opens up a way to obtain perfect n-type or p-type 2D materials with tunable carrier concentration and mobility, suitable for integrated circuit and optoelectronic device fabrication.

METHODS

The calculations were performed using the density functional theory (DFT),^{23,24} as implemented in the VASP codes.^{25,26} The electron exchange and correlation were treated using the Perdew–Burke–Ernzerhof functional.²⁷ The $6 \times 6 \times 1$ supercell was used for BN and graphene. The lateral lattice constant of BN was strained by -1.7% , to meet the commensurability criterion. An in-plane strain of roughly $+1.5\%$ was applied to BN for the heterostructure of $4 \times 4 \text{ MoS}_2$ - $5 \times 5 \text{ BN}$ supercell. The $2 \sqrt{3} \times 2 \sqrt{3} \text{ ZrS}_2$ supercell is strained by 0.2% to match the $4 \times 4 \text{ MoS}_2$ in the heterostructure of $\text{ZrS}_2/\text{MoS}_2$. The cell size in the z-direction is 20 \AA for the BN/graphene and BN/ MoS_2 and increases to 23 \AA for the systems of BN/BN/graphene and $\text{ZrS}_2/\text{MoS}_2$. All atoms are relaxed until the Hellmann–Feynman forces on individual atoms are no greater than 0.02 eV/\AA . The cutoff energy of the plane wave basis is 520 eV . The $3 \times 3 \times 1$ and $2 \times 2 \times 1$ Monkhorst–Pack mesh grids were used for the k-point sampling of the heterostructure of BN/ MoS_2 and other systems. The effects of spin polarization were included in all

calculations. The Grimme DFT-D2 method was used for correcting the van der Waals interactions.²⁸

RESULTS AND DISCUSSION

We start by validating the doping strategy on the heterostructure of defective BN and perfect graphene (BN/graphene). Here, the defects in BN are boron vacancy (V_B) and nitrogen vacancy (V_N) since they can be preferentially formed under an electron beam,²⁹ but the doping strategy is not limited to vacancies. Figure 1 involves the band structure comparison between V_B in the free-standing BN and V_B in BN/graphene heterostructure. V_B induces one spin-up defect state denoted as $d1_{up}$ and two spin-down defect states marked as $d1_{dn}$ and $d2_{dn}$ within the band gap in the free-standing BN, as shown in Figure 1a. They are all above the Fermi level and thus empty. However, we find that the $d1_{up}$ becomes occupied, and the Fermi level shifts below the Dirac cone of the graphene layer in BN/graphene, as shown in Figure 1b, demonstrating the charge of electron transfer from graphene to the $d1_{up}$ state and hence achieving the perfect p-type graphene without inducing any defects in it.

Since electronic devices are often bipolar,^{30–32} which necessitates the critical ability to dope the material sufficiently both p- and n-types, we also examine the inverse charge transfer, that is, from the defect in the BN layer to graphene, as shown in Figure 2 where the defect is V_N . For V_N , there is one filled spin-up state ($d1_{up}$) below the Fermi level and one empty spin-down state ($d1_{dn}$) above the Fermi level in the free-standing BN, whereas they become degenerate, locating above the Fermi level and being empty in BN/graphene, see the $d1$ state in Figure 2b. This is ascribed to the charge transfer from the $d1_{up}$ state to graphene, which at the same time moves the Fermi level above the Dirac cone of the graphene. Since oxygen often exists during the graphene synthesis process, we also placed one bridge oxygen atom on the graphene surface in the heterostructure of defective BN/graphene and found the oxygen adsorption has negligible

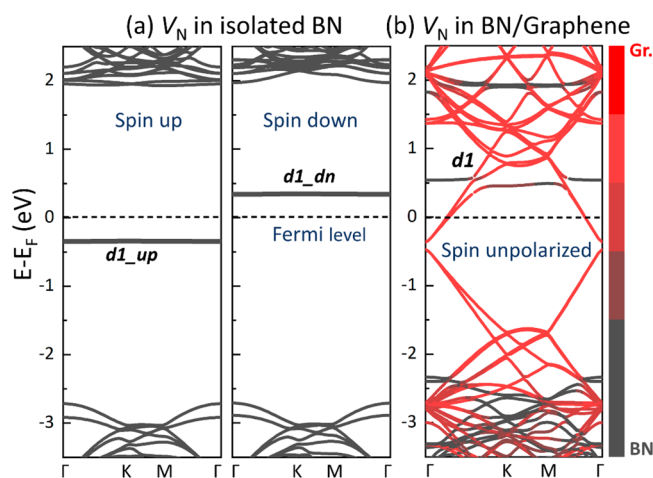


Figure 2. (a) Band structure of V_N in isolated BN. (b) Projected band structure of V_N in the heterostructure of BN/Graphene with red and black colors indicating weights of graphene and BN atomic orbital projections. The thick lines stand for the defect states induced around the Fermi level as indicated by the 0-eV line.

effects on the charge transfer between the V_B/V_N and the graphene (see Figures S1 and S2 in the Supporting Information). It should be noted that for free-standing BN, both nitrogen and boron vacancies are very deep defects with an ionization energy of more than 1 eV;¹⁸ thus, they are usually considered to be useless to offer an effective concentration of carriers for their parent material. However, now they can act as shallow donors and acceptors in the heterostructure by providing carriers to graphene. Moreover, we got the perfect n-type graphene in the heterostructure of defective BN/graphene with a point defect complex, in which a nitrogen vacancy is coupled to a nitrogen antisite defect ($N_B V_N$) in the BN layer, revealing that the defect complex is also able to realize the charge transfer (see Figure S3 in the Supporting Information).

It should be pointed out that in the heterostructure, the electron (or hole) and ionized V_N (or V_B) are confined into two different adjacent layers, allowing a remarkable reduction in the influence of ionized defect scattering,^{33,34} which is supposed to be the most critical cause for low carrier mobility in the 2D devices.^{35,36} To further suppress the Coulomb effects of the ionized defects, we increase the spatial separation between the ionized defects and the carriers by inserting one more perfect BN layer between the defective BN and the graphene. The insertion of the perfect BN layer leads to a lower charge transfer efficiency but can still be effective to offer carriers, as shown in Figure 3. On the basis of Bader analysis, the electrons and holes transferred from V_N and V_B to graphene in the system of defective BN/perfect BN/graphene are 57% and 77% of those in the system of defective BN/graphene. Meanwhile, the Fermi level shifts relative to the Dirac cone of the graphene are smaller because of the insertion of the extra BN layer. More interestingly, the percentage further drops to 35% and 63% when the perfect BN layer is removed, but the distance between the defective BN and graphene is kept. This reveals the insertion of the perfect BN layer is like putting a “ladder” between the defective BN and graphene separated by a long distance, which makes it easier for the charges in the defective BN to land the graphene (see Figures S4 and S5 in the Supporting Information for details). These results indicate the carrier density and mobility in this

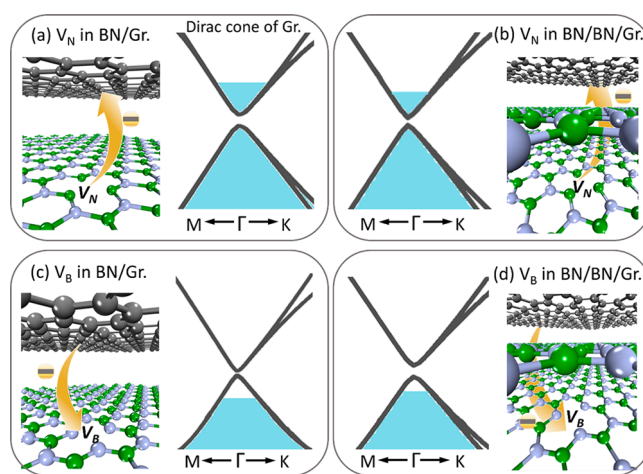


Figure 3. Comparison of the charge transfer in defective BN/graphene (a) and (c), and defective BN/perfect BN/graphene (b) and (d). In each figure, one side shows the schematic diagrams of the electron transfer from the native defect (V_N or V_B) in BN to graphene (Gr.) and the other side shows the Dirac cone of the graphene. The blue color shows the electron occupation. Light blue, green, and gray balls are N, B, and C atoms, respectively.

heterostructure doping strategy can be tuned by engineering the surrounding environment.

To extend the doping strategy to other 2D materials with a significant band gap, we also put the defective BN (with V_N) and one perfect MoS_2 layer together, aiming to achieve the n-type doping of MoS_2 , which is one of the most extensively studied 2D systems.^{37,38} Figure 4 shows the band structure of V_N in BN/ MoS_2 , wherein the defect state ($d1$, blue line) is above the Fermi level and across the lowest conduction band of MoS_2 (purple line). The electronic wave functions of the two states are shown in the inset of Figure 4. This means the

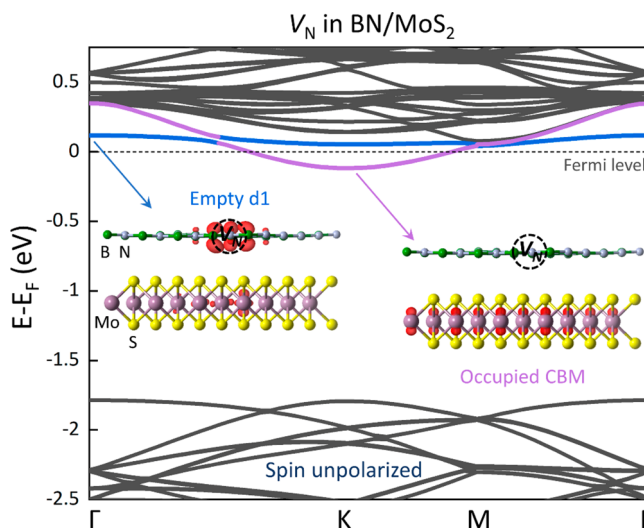


Figure 4. Band structure of V_N in BN/ MoS_2 . The blue line is the defect level from which the electron is transferred to the lowest conduction band of MoS_2 , which is denoted by the purple line. Insets show the electronic wave functions associated with the Γ point of the blue line and K point of the purple line (i.e. the conduction band minimum (CBM)) with red-color isosurfaces at $0.0025 \text{ e}/\text{\AA}^3$. The Fermi level is indicated by the 0-eV line. Light blue, green, purple, and yellow balls are N, B, Mo, and S atoms, respectively.

electron originally occupying the dI_{up} state in isolated BN (see Figure 2a) has transferred to the lowest conduction band of MoS_2 , resulting in a perfect n-type MoS_2 .

MoS_2 has been reported to exhibit the unipolar characteristic and the achievement of p-type MoS_2 is a challenge.^{39,40} With the modulation doping strategy, we gain a perfect p-type MoS_2 in the heterostructure of defective ZrS_2/MoS_2 . Figure 5a,b

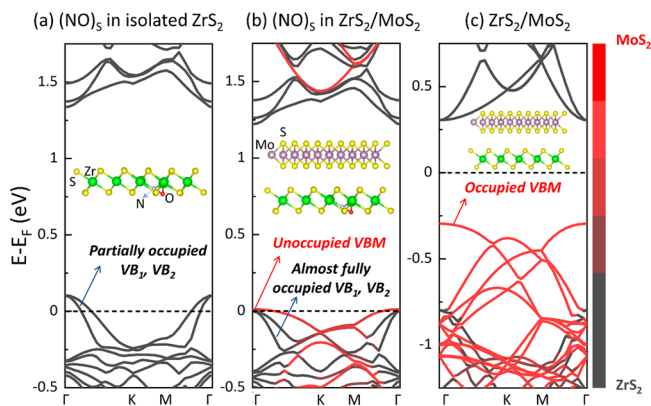


Figure 5. (a) Band structure of $(NO)_S$ in isolated ZrS_2 . (b) Projected band structure of $(NO)_S$ in the heterostructure of ZrS_2/MoS_2 . (c) Projected band structure of the heterostructure of perfect ZrS_2/MoS_2 . Red and black colors in (b) and (c) indicate weights of MoS_2 and ZrS_2 atomic orbital projections. The inset figures show the corresponding atomic structures. The Fermi level is indicated by the 0-eV line. Bright green, purple, yellow, light blue, and red balls are Zr, Mo, S, N, and O atoms, respectively.

show the band structure comparison between the defect ($(NO)_S$, one NO molecule adsorbed on one sulfur vacancy) in free-standing ZrS_2 and $(NO)_S$ in ZrS_2/MoS_2 heterostructure. The $(NO)_S$ introduces no defect states within the band gap of ZrS_2 but moves the top two valence band-edge states up across the Fermi level, making them partially occupied, as shown in Figure 5a. The partially occupied valence bands become almost fully occupied in the defective ZrS_2/MoS_2 heterostructure, and the valence band maximum (VBM) of MoS_2 gets unoccupied, as shown in Figure 5b, revealing the electron transfer from MoS_2 to the defective ZrS_2 and the realization of the perfect p-type MoS_2 . It is important to emphasize that this charge transfer is impossible to occur in perfect ZrS_2/MoS_2 heterostructure, the band structure of which is shown in Figure 5c. The defects in BN described in the systems of BN/graphene and BN/ MoS_2 act as the source of electrons and holes for doping graphene or MoS_2 , whereas, in this circumstance, the defect in ZrS_2 is not directly involved in the charge transfer process but plays an essential role in modifying the occupation of band-edge states of the encapsulation layer and then promoting the charge transfer. For MoS_2 , most of the experimentally reported mobilities are much smaller than the theoretically predicted value and one of the reasons for the discrepancy is believed to be the Coulomb impurities scattering.^{35,41} In principle, our proposed strategy is advantageous in improving the experimental mobility because of the significant suppression of the Coulomb impurities scattering inside the MoS_2 . The doping strategy is not unique to a certain 2D material, but can be readily applied for any other 2D material, as we have demonstrated for both zero-bandgap graphene and the semiconducting MoS_2 . This is of particular importance since the strong Coulomb impurities

scattering is inevitable if one follows the traditional way of doping in 3D semiconductors wherein the defects are created inside the channel layer.

It would also be straightforward for this doping strategy to be implemented in experiments, since the techniques of synthesizing 2D heterostructures (such as mechanical exfoliation,⁴² molecular-beam epitaxy,⁴³ and chemical vapor deposition⁴⁴) and fabrication of 2D devices with an encapsulated material on the channel layer^{45–48} have been widely reported. Meanwhile, it is recommended to choose easy-to-formed defects for the encapsulation layer, such as vacancies (usual products of electron-beam irradiation⁴⁹) or defects that can be simply obtained by adjusting the growth environment of the 2D material. To be specific, a chalcogen vacancy and a transition metal vacancy are usually observed in transition metal dichalcogenides,^{50–53} and oxygen-related defects can be easily introduced into black phosphorus since it has a high sensitivity to oxygen.⁵⁴ Although the irradiation may induce unintentional damage, this only happens to the encapsulation layer but not the channel layer. The energy of the electron beam can also be a way to engineer the defects in the encapsulation layer and thus the carrier concentration and mobility in the channel layer. Moreover, the van der Waals stacking of 2D materials is advantageous in designing intended properties, showing another engineering route. The strategy demonstrated hereby is not only effective to control the conductivity but also practical for the current 2D electronic material manufacturing process. In the current work, the channel layer is assumed to be perfect. For the channel material with unintentional defect, the defect may act as the acceptor of the electron/hole donated by the encapsulation layer. The system of defective BN/ MoS_2 with V_S (sulfur vacancy) is such an example, where the electron is transferred from V_N in BN to V_S in MoS_2 (see Figure S6a,b in the Supporting Information). Under this circumstance, providing a sulfur-rich condition to suppress V_S or exposing the sample in an oxygen-rich condition to passivate V_S would be the practical way to recover the charge transfer between the encapsulation layer and the band-edge states of the channel layer (see Figure S6c in the Supporting Information).

■ SUMMARY

In conclusion, we have proposed a doping strategy that depends on the charge transfer between the 2D channel layer and defects in the adjacent 2D encapsulation layer. The encapsulation layer allows no damage to the channel layer and the deep-level defects inside it play an important role in providing free carriers to the channel layer. The spatially separated carriers and ionized defects significantly suppress the Coulomb impurities scattering and thus improve the carrier mobility. The strategy is demonstrated for the cases of defective BN/graphene, defective BN/ MoS_2 , and defective ZrS_2/MoS_2 . It is also found that engineering the environmental screening of the defective encapsulation layer can tailor the carrier density. As an example, inserting one more perfect BN layer between the defective BN and graphene adjust the number of electrons transferred between them. The strategy could be widely used to produce other perfect n-type/p-type 2D materials with their original high mobility in channel materials retained, which will be a very promising way to overcome the current doping problem for 2D material electronics, such as in integrated circuits and optoelectronic devices.

■ ASSOCIATED CONTENT

SI Supporting Information

The Supporting Information is available free of charge at <https://pubs.acs.org/doi/10.1021/acs.nanolett.1c02192>.

Oxygen adsorption on graphene in defective BN/graphene, a point defect complex in BN/graphene, charge transfer efficiency between defective BN and graphene, nitrogen vacancy in BN/MoS₂ (with V_S and O_S in MoS₂) (PDF)

■ AUTHOR INFORMATION

Corresponding Authors

Xian-Bin Li – State Key Laboratory of Integrated Optoelectronics, College of Electronic Science and Engineering, Jilin University, Changchun 130012, China; orcid.org/0000-0002-0046-2016; Email: lixianbin@jlu.edu.cn

Hong-Bo Sun – State Key Laboratory of Integrated Optoelectronics, College of Electronic Science and Engineering, Jilin University, Changchun 130012, China; State Key Laboratory of Precision Measurement Technology and Instruments, Department of Precision Instrument, Tsinghua University, Beijing 100084, China; Email: hbsun@tsinghua.edu.cn

Author

Dan Wang – State Key Laboratory of Integrated Optoelectronics, College of Electronic Science and Engineering, Jilin University, Changchun 130012, China; Department of Materials Science and Engineering, Rensselaer Polytechnic Institute, Troy, New York 12180, United States

Complete contact information is available at: <https://pubs.acs.org/10.1021/acs.nanolett.1c02192>

Author Contributions

D.W. performed the calculations, and D.W. and X.-B.L. conducted the theoretical analyses. The paper was written by D.W. and X.-B.L. with the help from all the authors. All the authors contributed to the interpretation of the results. X.-B.L. and H.-B.S. conceived the initial idea for this research.

Notes

The authors declare no competing financial interest.

■ ACKNOWLEDGMENTS

X.-B.L. thanks the support of National Natural Science Foundation of China (Nos. 61922035 and 11874171) and the Fundamental Research Funds for the Central Universities. The High-performance Computing Center (HPCC) of Jilin University is also acknowledged for the calculation resources.

■ REFERENCES

- (1) Lee, S.-J.; Lin, Z.; Duan, X.; Huang, Y. Doping on Demand in 2D Devices. *Nat. Electron* **2020**, *3* (2), 77–78.
- (2) Wang, D.; Li, X.-B.; Han, D.; Tian, W. Q.; Sun, H.-B. Engineering Two-Dimensional Electronics by Semiconductor Defects. *Nano Today* **2017**, *16*, 30–45.
- (3) Akinwande, D.; Huyghebaert, C.; Wang, C.-H.; Serna, M. I.; Goossens, S.; Li, L.-J.; Wong, H.-S. P.; Koppens, F. H. L. Graphene and Two-Dimensional Materials for Silicon Technology. *Nature* **2019**, *573* (7775), 507–518.
- (4) Efetov, D. K.; Kim, P. Controlling Electron-Phonon Interactions in Graphene at Ultrahigh Carrier Densities. *Phys. Rev. Lett.* **2010**, *105* (25), 256805.

(5) Williams, J. R.; DiCarlo, L.; Marcus, C. M. Quantum Hall Effect in a Gate-Controlled p-n Junction of Graphene. *Science* **2007**, *317* (5838), 638–641.

(6) Cai, B.; Zhang, S.; Yan, Z.; Zeng, H. Noncovalent Molecular Doping of Two-Dimensional Materials. *ChemNanoMat* **2015**, *1* (8), 542–557.

(7) Luo, P.; Zhuge, F.; Zhang, Q.; Chen, Y.; Lv, L.; Huang, Y.; Li, H.; Zhai, T. Doping Engineering and Functionalization of Two-Dimensional Metal Chalcogenides. *Nanoscale Horiz.* **2019**, *4* (1), 26–51.

(8) Cristoloveanu, S.; Lee, K. H.; Park, H.; Parihar, M. S. The Concept of Electrostatic Doping and Related Devices. *Solid-State Electron.* **2019**, *155*, 32–43.

(9) Li, T.; Mao, D.; Petrone, N. W.; Grassi, R.; Hu, H.; Ding, Y.; Huang, Z.; Lo, G.-Q.; Hone, J. C.; Low, T.; Wong, C. W.; Gu, T. Spatially Controlled Electrostatic Doping in Graphene P-i-n Junction for Hybrid Silicon Photodiode. *npj 2D Materials and Applications* **2018**, *2* (1), 1–8.

(10) Kwon, S.-J.; Han, T.-H.; Ko, T. Y.; Li, N.; Kim, Y.; Kim, D. J.; Bae, S.-H.; Yang, Y.; Hong, B. H.; Kim, K. S.; Ryu, S.; Lee, T.-W. Extremely Stable Graphene Electrodes Doped with Macromolecular Acid. *Nat. Commun.* **2018**, *9* (1), 2037.

(11) Iberi, V.; Liang, L.; Ievlev, A. V.; Stanford, M. G.; Lin, M.-W.; Li, X.; Mahjouri-Samani, M.; Jesse, S.; Sumpster, B. G.; Kalinin, S. V.; Joy, D. C.; Xiao, K.; Belianinov, A.; Ovchinnikova, O. S. Nanoforging Single Layer MoSe₂ Through Defect Engineering with Focused Helium Ion Beams. *Sci. Rep.* **2016**, *6* (1), 30481.

(12) Xu, K.; Zhao, Y.; Lin, Z.; Long, Y.; Wang, Y.; Chan, M.; Chai, Y. Doping of Two-Dimensional MoS₂ by High Energy Ion Implantation. *Semicond. Sci. Technol.* **2017**, *32* (12), 124002.

(13) Smart, T. J.; Wu, F.; Govoni, M.; Ping, Y. Fundamental Principles for Calculating Charged Defect Ionization Energies in Ultrathin Two-Dimensional Materials. *Physical Review Materials* **2018**, *2* (12), 124002.

(14) Wang, D.; Sundararaman, R. Substrate Effects on Charged Defects in Two-Dimensional Materials. *Phys. Rev. Materials* **2019**, *3* (8), No. 083803.

(15) Ma, J.; Yu, Z. G.; Zhang, Y.-W. Tuning Deep Dopants to Shallow Ones in 2D Semiconductors by Substrate Screening: The Case of X_S (X = Cl, Br, I) in MoS₂. *Phys. Rev. B* **2017**, *95* (16), 165447.

(16) Wang, D.; Sundararaman, R. Layer Dependence of Defect Charge Transition Levels in Two-Dimensional Materials. *Phys. Rev. B* **2020**, *101* (5), No. 054103.

(17) Guo, C.; Xu, J.; Rocca, D.; Ping, Y. Substrate Screening Approach for Quasiparticle Energies of Two-Dimensional Interfaces with Lattice Mismatch. *Phys. Rev. B* **2020**, *102* (20), 205113.

(18) Wang, D.; Han, D.; Li, X.-B.; Xie, S.-Y.; Chen, N.-K.; Tian, W. Q.; West, D.; Sun, H.-B.; Zhang, S. B. Determination of Formation and Ionization Energies of Charged Defects in Two-Dimensional Materials. *Phys. Rev. Lett.* **2015**, *114* (19), 196801.

(19) Zhang, S. B. The Microscopic Origin of the Doping Limits in Semiconductors and Wide-Gap Materials and Recent Developments in Overcoming These Limits: A Review. *J. Phys.: Condens. Matter* **2002**, *14* (34), R881–R903.

(20) Huang, B.; Yoon, M.; Sumpster, B. G.; Wei, S.-H.; Liu, F. Alloy Engineering of Defect Properties in Semiconductors: Suppression of Deep Levels in Transition-Metal Dichalcogenides. *Phys. Rev. Lett.* **2015**, *115* (12), 126806.

(21) Li, M.-Y.; Su, S.-K.; Wong, H.-S. P.; Li, L.-J. How 2D Semiconductors Could Extend Moore's Law. *Nature* **2019**, *567* (7747), 169–170.

(22) Su, S.-K.; Chuu, C.-P.; Li, M.-Y.; Cheng, C.-C.; Wong, H.-S. P.; Li, L.-J. Layered Semiconducting 2D Materials for Future Transistor Applications. *Small Structures* **2021**, *2* (5), 2000103.

(23) Kohn, W.; Sham, L. J. Self-Consistent Equations Including Exchange and Correlation Effects. *Phys. Rev.* **1965**, *140* (4A), A1133–A1138.

- (24) Hohenberg, P.; Kohn, W. Inhomogeneous Electron Gas. *Phys. Rev.* **1964**, *136* (3B), B864–B871.
- (25) Kresse, G.; Furthmüller, J. Efficiency of Ab-Initio Total Energy Calculations for Metals and Semiconductors Using a Plane-Wave Basis Set. *Comput. Mater. Sci.* **1996**, *6* (1), 15–50.
- (26) Kresse, G.; Furthmüller, J. Efficient Iterative Schemes for Ab Initio Total-Energy Calculations Using a Plane-Wave Basis Set. *Phys. Rev. B* **1996**, *54* (16), 11169–11186.
- (27) Perdew, J. P.; Burke, K.; Ernzerhof, M. Generalized Gradient Approximation Made Simple. *Phys. Rev. Lett.* **1996**, *77* (18), 3865–3868.
- (28) Grimme, S. Semiempirical GGA-type density functional constructed with a long-range dispersion correction. *J. Comput. Chem.* **2006**, *27* (15), 1787–1799.
- (29) Dogan, M.; Gilbert, S. M.; Pham, T.; Shevitski, B.; Ercius, P.; Aloni, S.; Zettl, A.; Cohen, M. L. Electron Beam-Induced Nanopores in Bernal-Stacked Hexagonal Boron Nitride. *Appl. Phys. Lett.* **2020**, *117* (2), No. 023102.
- (30) Asbeck, P. M.; Chang, F. M.; Wang, K.; Sullivan, G. J.; Cheung, D. T. GaAs-Based Heterojunction Bipolar Transistors for Very High Performance Electronic Circuits. *Proc. IEEE* **1993**, *81* (12), 1709–1726.
- (31) Lucas, R. A.; Lin, C.-Y.; Baker, L. A.; Siwy, Z. S. Ionic Amplifying Circuits Inspired by Electronics and Biology. *Nat. Commun.* **2020**, *11* (1), 1568.
- (32) Tybrandt, K.; Gabrielsson, E. O.; Berggren, M. Toward Complementary Ionic Circuits: The npn Ion Bipolar Junction Transistor. *J. Am. Chem. Soc.* **2011**, *133* (26), 10141–10145.
- (33) Dingle, R.; Störmer, H. L.; Gossard, A. C.; Wiegmann, W. Electron Mobilities in Modulation-doped Semiconductor Heterojunction Superlattices. *Appl. Phys. Lett.* **1978**, *33* (7), 665–667.
- (34) People, R.; Bean, J. C.; Lang, D. V.; Sergent, A. M.; Störmer, H. L.; Wecht, K. W.; Lynch, R. T.; Baldwin, K. Modulation Doping in Ge_xSi_{1-x}/Si Strained Layer Heterostructures. *Appl. Phys. Lett.* **1984**, *45* (11), 1231–1233.
- (35) Yu, Z.; Ong, Z.-Y.; Pan, Y.; Cui, Y.; Xin, R.; Shi, Y.; Wang, B.; Wu, Y.; Chen, T.; Zhang, Y.-W.; Zhang, G.; Wang, X. Realization of Room-Temperature Phonon-Limited Carrier Transport in Monolayer MoS₂ by Dielectric and Carrier Screening. *Adv. Mater.* **2016**, *28* (3), 547–552.
- (36) Ma, N.; Jena, D. Charge Scattering and Mobility in Atomically Thin Semiconductors. *Phys. Rev. X* **2014**, *4* (1), No. 011043.
- (37) Wang, D.; Han, D.; West, D.; Chen, N.-K.; Xie, S.-Y.; Tian, W. Q.; Meunier, V.; Zhang, S.; Li, X.-B. Excitation to Defect-Bound Band Edge States in Two-Dimensional Semiconductors and Its Effect on Carrier Transport. *npj Computational Materials* **2019**, *5* (1), 8.
- (38) Wang, L.; Wang, Z.; Wang, H.-Y.; Grinblat, G.; Huang, Y.-L.; Wang, D.; Ye, X.-H.; Li, X.-B.; Bao, Q.; Wee, A.-S.; Maier, S. A.; Chen, Q.-D.; Zhong, M.-L.; Qiu, C.-W.; Sun, H.-B. Slow Cooling and Efficient Extraction of C-Exciton Hot Carriers in MoS₂ Monolayer. *Nat. Commun.* **2017**, *8* (1), 13906.
- (39) Li, M.; Yao, J.; Wu, X.; Zhang, S.; Xing, B.; Niu, X.; Yan, X.; Yu, Y.; Liu, Y.; Wang, Y. P-Type Doping in Large-Area Monolayer MoS₂ by Chemical Vapor Deposition. *ACS Appl. Mater. Interfaces* **2020**, *12* (5), 6276–6282.
- (40) Choi, M. Strain-Enhanced p Doping in Monolayer MoS₂. *Phys. Rev. Appl.* **2018**, *9* (2), No. 024009.
- (41) Qiu, H.; Xu, T.; Wang, Z.; Ren, W.; Nan, H.; Ni, Z.; Chen, Q.; Yuan, S.; Miao, F.; Song, F.; Long, G.; Shi, Y.; Sun, L.; Wang, J.; Wang, X. Hopping Transport through Defect-Induced Localized States in Molybdenum Disulphide. *Nat. Commun.* **2013**, *4* (1), 2642.
- (42) Li, M.-Y.; Chen, C.-H.; Shi, Y.; Li, L.-J. Heterostructures Based on Two-Dimensional Layered Materials and Their Potential Applications. *Mater. Today* **2016**, *19* (6), 322–335.
- (43) Diaz, H. C.; Chaghi, R.; Ma, Y.; Batzill, M. Molecular Beam Epitaxy of the van Der Waals Heterostructure MoTe₂ on MoS₂: Phase, Thermal, and Chemical Stability. *2D Mater.* **2015**, *2* (4), No. 044010.
- (44) Cai, Z.; Liu, B.; Zou, X.; Cheng, H.-M. Chemical Vapor Deposition Growth and Applications of Two-Dimensional Materials and Their Heterostructures. *Chem. Rev.* **2018**, *118* (13), 6091–6133.
- (45) Shi, W.; Kahn, S.; Jiang, L.; Wang, S.-Y.; Tsai, H.-Z.; Wong, D.; Taniguchi, T.; Watanabe, K.; Wang, F.; Crommie, M. F.; Zettl, A. Reversible Writing of High-Mobility and High-Carrier-Density Doping Patterns in Two-Dimensional van Der Waals Heterostructures. *Nature Electronics* **2020**, *3* (2), 99–105.
- (46) Lee, G.-H.; Cui, X.; Kim, Y. D.; Arefe, G.; Zhang, X.; Lee, C.-H.; Ye, F.; Watanabe, K.; Taniguchi, T.; Kim, P.; Hone, J. Highly Stable, Dual-Gated MoS₂ Transistors Encapsulated by Hexagonal Boron Nitride with Gate-Controllable Contact, Resistance, and Threshold Voltage. *ACS Nano* **2015**, *9* (7), 7019–7026.
- (47) Rai, A.; Valsaraj, A.; Movva, H. C. P.; Roy, A.; Ghosh, R.; Sonde, S.; Kang, S.; Chang, J.; Trivedi, T.; Dey, R.; Guchhait, S.; Larentis, S.; Register, L. F.; Tutuc, E.; Banerjee, S. K. Air Stable Doping and Intrinsic Mobility Enhancement in Monolayer Molybdenum Disulfide by Amorphous Titanium Suboxide Encapsulation. *Nano Lett.* **2015**, *15* (7), 4329–4336.
- (48) Zhang, Z.; Wang, Z.; Shi, T.; Bi, C.; Rao, F.; Cai, Y.; Liu, Q.; Wu, H.; Zhou, P. Memory Materials and Devices: From Concept to Application. *InfoMat* **2020**, *2* (2), 261–290.
- (49) Jiang, J.; Xu, T.; Lu, J.; Sun, L.; Ni, Z. Defect Engineering in 2D Materials: Precise Manipulation and Improved Functionalities. *Research* **2019**, *2019*, 1–14.
- (50) Hong, J.; Hu, Z.; Probert, M.; Li, K.; Lv, D.; Yang, X.; Gu, L.; Mao, N.; Feng, Q.; Xie, L.; Zhang, J.; Wu, D.; Zhang, Z.; Jin, C.; Ji, W.; Zhang, X.; Yuan, J.; Zhang, Z. Exploring Atomic Defects in Molybdenum Disulphide Monolayers. *Nat. Commun.* **2015**, *6* (1), 6293.
- (51) Zhou, W.; Zou, X.; Najmaei, S.; Liu, Z.; Shi, Y.; Kong, J.; Lou, J.; Ajayan, P. M.; Yakobson, B. I.; Idrobo, J.-C. Intrinsic Structural Defects in Monolayer Molybdenum Disulfide. *Nano Lett.* **2013**, *13* (6), 2615–2622.
- (52) Zhang, S.; Wang, C.-G.; Li, M.-Y.; Huang, D.; Li, L.-J.; Ji, W.; Wu, S. Defect Structure of Localized Excitons in a WSe₂ Monolayer. *Phys. Rev. Lett.* **2017**, *119* (4), No. 046101.
- (53) Nguyen, L.; Komsa, H.-P.; Khestanova, E.; Kashtiban, R. J.; Peters, J. J. P.; Lawlor, S.; Sanchez, A. M.; Sloan, J.; Gorbachev, R. V.; Grigorieva, I. V.; Krashennnikov, A. V.; Haigh, S. J. Atomic Defects and Doping of Monolayer NbSe₂. *ACS Nano* **2017**, *11* (3), 2894–2904.
- (54) Kumar, A.; Telesio, F.; Forti, S.; Al-Temimy, A.; Coletti, C.; Serrano-Ruiz, M.; Caporali, M.; Peruzzini, M.; Beltram, F.; Heun, S. STM Study of Exfoliated Few Layer Black Phosphorus Annealed in Ultrahigh Vacuum. *2D Mater.* **2019**, *6* (1), No. 015005.

Supporting Information for
Modulation Doping: A Strategy for 2D Materials Electronics

Dan Wang^{1,2}, Xian-Bin Li^{1*}, and Hong-Bo Sun^{1,3*}

¹*State Key Laboratory of Integrated Optoelectronics, College of Electronic Science and Engineering, Jilin University, Changchun 130012, China*

²*Department of Materials Science and Engineering, Rensselaer Polytechnic Institute, 110 8th Street, Troy, New York 12180, USA*

³*State Key Laboratory of Precision Measurement Technology and Instruments, Department of Precision Instrument, Tsinghua University, Beijing 100084, China*

E-mail: lixianbin@jlu.edu.cn (X.-B. Li), hbsun@tsinghua.edu.cn (H.-B. S)

1. Oxygen adsorption on graphene in defective BN/graphene

Fig. S1 shows the band structure comparison of the V_B in BN/graphene and the V_B in BN/graphene with O_i (one oxygen is adsorbed on the bridge site of graphene). In both cases, the $d1_up$ state is occupied and the Fermi level is below the Dirac cone of graphene, indicating the charge transfer between $d1_up$ of V_B in BN and the graphene is not affected by the existence of O_i . Also, the inverse charge transfer from V_N in BN to graphene keeps successful before and after the bridge oxygen is adsorbed on graphene, as shown in Fig. S2.

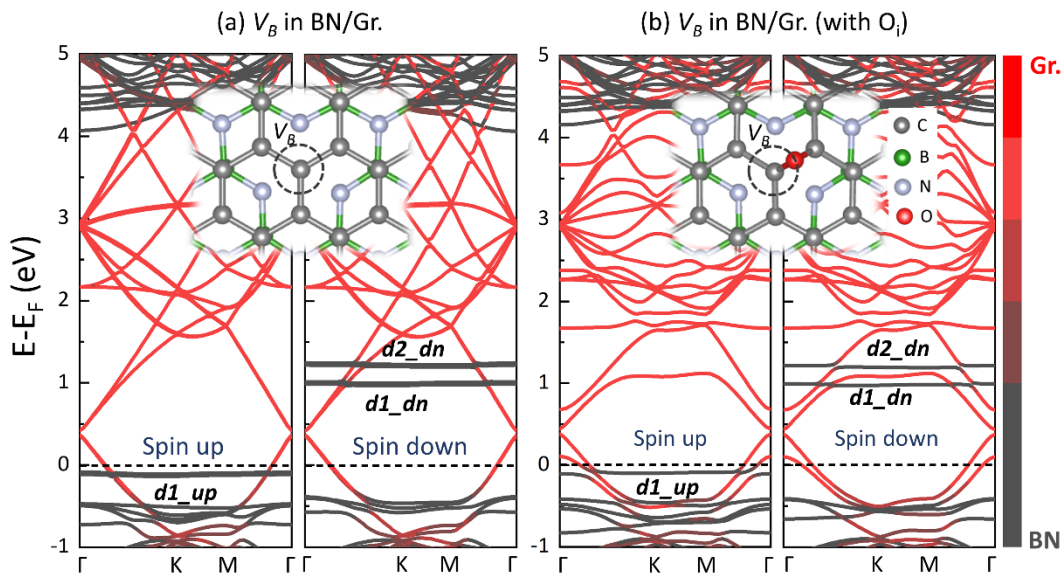


Figure S1 Projected band structure of (a) BN/graphene with V_B (one boron vacancy) in BN and (b) BN/graphene with V_B in BN and O_i (one epoxy group, i.e., bridge oxygen) in graphene. The red and black colors indicating weights of graphene and BN atomic orbital projections. The Fermi level is indicated by the 0-eV line. The inset figures show the corresponding atomic structures. Light blue, green, gray, and red balls are N, B, C, and O atoms, respectively.

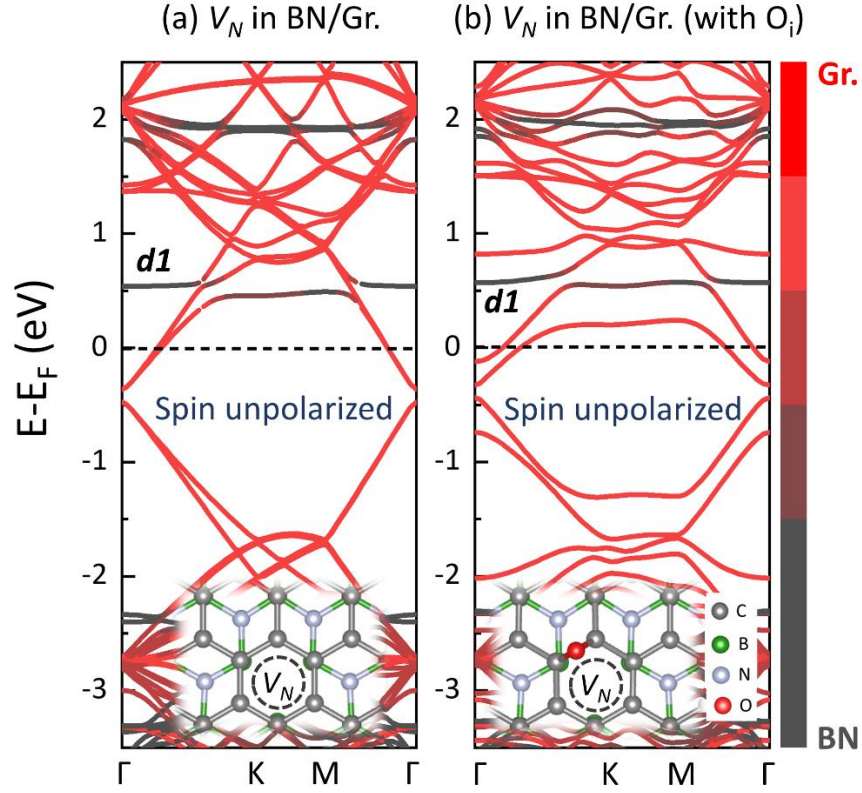


Figure S2 Projected band structure of (a) BN/graphene with V_N (one boron vacancy) in BN and (b) BN/graphene with V_N in BN and O_i (one epoxy group, i.e., bridge oxygen) in graphene. The red and black colors indicating weights of graphene and BN atomic orbital projections. The Fermi level is indicated by the 0-eV line. The inset figures show the corresponding atomic structures. Light blue, green, gray, and red balls are N, B, C, and O atoms, respectively.

2. A point defect complex in BN/graphene

We can also achieve the perfect n-type graphene in the heterostructure of defective BN/graphene with a point defect complex, in which a nitrogen vacancy is coupled to a nitrogen anti-site defect ($N_B V_N$) in the BN layer, as shown in Fig. S3. $N_B V_N$ in isolated BN induces three spin-up and spin-down states within the band gap, among which the $d2_{up}$ is fully occupied. The $d2_{up}$ becomes partially occupied in the heterostructure of BN/graphene and the Fermi level shifts above the Dirac cone of graphene, revealing a charge transfer from the $d2_{up}$ of $N_B V_N$ in BN to the graphene and hence achieving an n-type graphene.

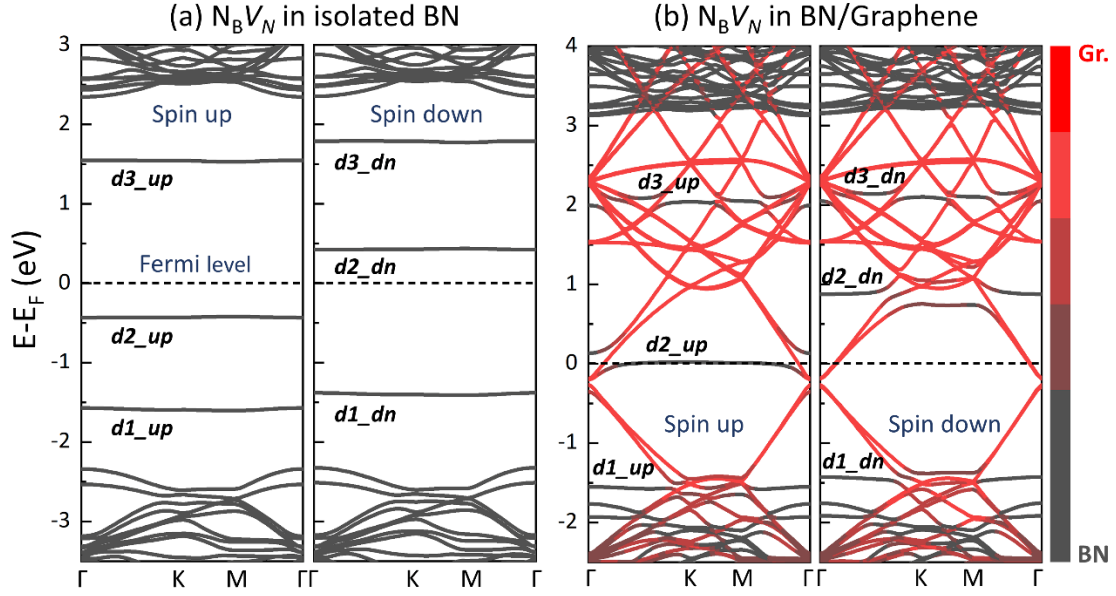


Figure S3 (a) Band structure of $N_B V_N$ in isolated BN. (b) Projected band structure of $N_B V_N$ in the heterostructure of BN/Graphene with red and black colors indicating weights of graphene and BN atomic orbital projections. The Fermi level is indicated by the 0-eV line.

3. Charge transfer efficiency between defective BN and graphene

Figs. S4 and S5 show the projected band structure of defective BN/graphene, defective BN/perfect BN/graphene, and defective BN/graphene with a large interlayer spacing (same with that between the defective BN and graphene in the system of defective BN/perfect BN/graphene). The defects in BN are V_N and V_B , respectively. Based on Bader analysis, the number of electrons transferred between the defective BN and graphene in such three systems are in descending order, as labeled at the bottom of the figures.

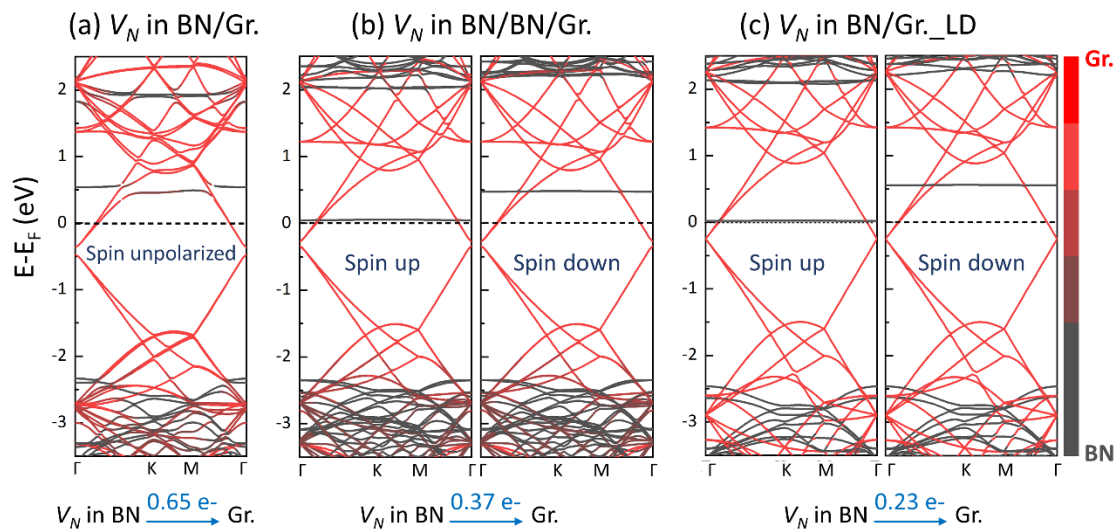


Figure S4 Projected band structure of (a) defective BN/graphene, (b) defective BN/perfect BN/graphene, and (c) defective BN/graphene with large interlayer distance (same with that between the defective BN and graphene in the system of defective BN/perfect BN/graphene). The defect is V_N . Red and black colors indicate weights of graphene and BN (including both defective and perfect layers) atomic orbital projections. The Fermi level is indicated by the 0-eV line. The number of transferred electrons is shown at the bottom.

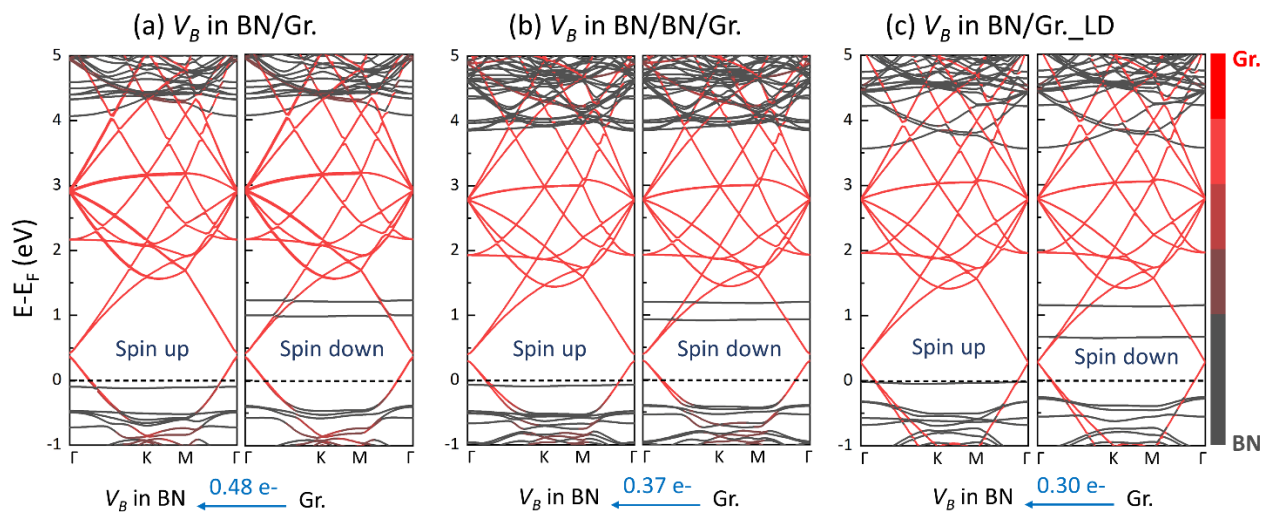


Figure S5 Projected band structure of (a) defective BN/graphene, (b) defective BN/perfect BN/graphene, and (c) defective BN/graphene with large interlayer distance (same with that between the defective BN and graphene in the system of defective BN/perfect BN/graphene). The defect is V_B . Red and black colors indicate weights of graphene and BN (including both defective and perfect layers) atomic orbital projections. The Fermi level is indicated by the 0-eV line. The number of transferred electrons is shown at the bottom.

4. V_N in BN/MoS₂ (with V_S and Os in MoS₂)

Fig. S6 (a) shows the band structure of V_N in BN/MoS₂. The blue line is the defect level of V_N from which the electron is transferred to the lowest conduction band of MoS₂ (the purple line), showing a perfect n-type MoS₂. The most common defect in MoS₂ is reported to be sulfur vacancy (V_S). To explore its influences on the charge transfer process, we introduce one V_S in the MoS₂ and calculate the band structure of the heterostructure, as shown in Fig. S6 (b). V_S induces three spin-up and spin-down states within the band gap (see the dotted lines), among which the green one (d2_up) is empty in isolated MoS₂¹ and becomes occupied in the heterostructure, proving charge transfer from the defect state d1_up of V_N (see Figure 2a in the main text) to d2_up of V_S . V_S can be easily passivated by oxygen atom both during material growth and exposure to ambient conditions²⁻⁵. The band structure of the heterostructure with oxygen passivation is shown in Fig. S6 (c), wherein, the gap states of V_S are disappeared and the lowest conduction band of MoS₂ successfully accepts the electron from V_N , showing an n-type MoS₂ again.

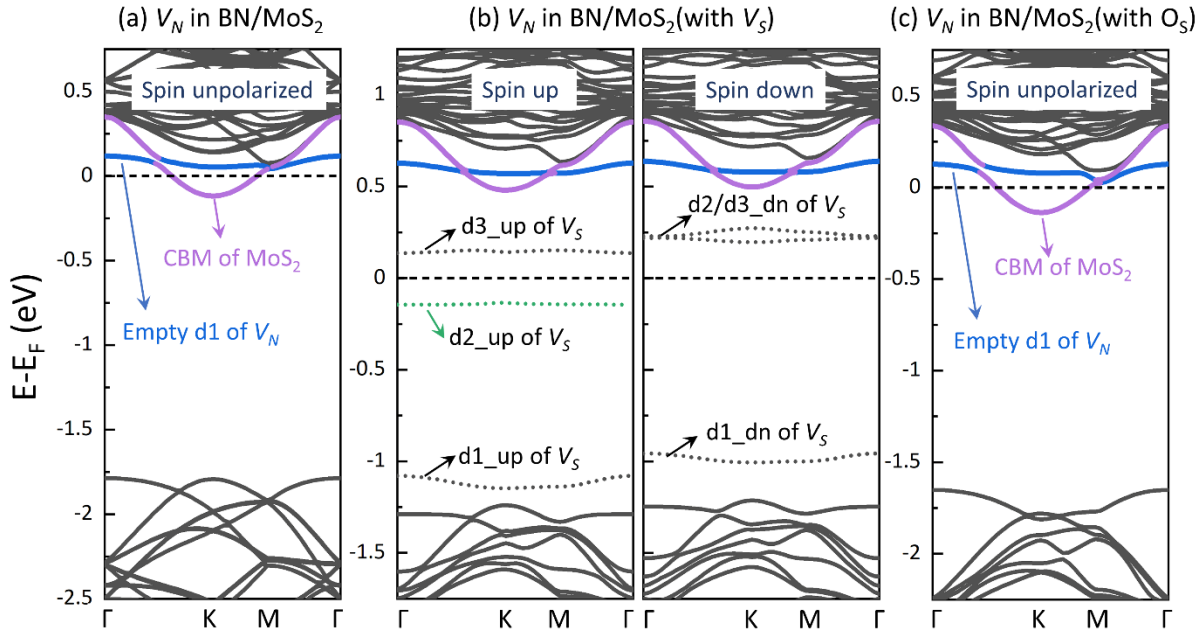


Figure S6 Band structure of (a) BN/MoS₂ with V_N (one nitrogen vacancy) in BN, (b) BN/MoS₂ with V_N in BN and V_S (one sulfur vacancy) in MoS₂, and (c) BN/MoS₂ with V_N in BN and one substitutional defect Os (one sulfur is replaced by one oxygen) in MoS₂. The blue line is the defect level of V_N , the purple line is the lowest conduction band of MoS₂, and the dotted lines in (b) are the defect levels of V_S . The Fermi level is indicated by the 0-eV line. CBM is short for conduction band minimum.

References

- (1) Naik, M. H.; Jain, M. Substrate Screening Effects on the Quasiparticle Band Gap and Defect Charge Transition Levels in MoS₂. *Phys. Rev. Materials* 2018, 2 (8), 084002.
- (2) Bretscher, H. M.; Li, Z.; Xiao, J.; Qiu, D. Y.; Refaely-Abramson, S.; Alexander-Webber, J.; Tanoh, A. O. A.; Fan, Y.; Delpont, G.; Williams, C.; Stranks, S. D.; Hofmann, S.; Neaton, J. B.; Louie, S. G.; Rao, A. The Bright Side of Defects in MoS₂ and WS₂ and a Generalizable Chemical Treatment Protocol for Defect Passivation. *arXiv:2002.03956* **2020**.
- (3) Pető, J. Spontaneous Doping of the Basal Plane of MoS₂ Single Layers through Oxygen Substitution under Ambient Conditions. *Nature Chemistry* **2018**, 10, 6.
- (4) Barja, S.; Refaely-Abramson, S.; Schuler, B.; Qiu, D. Y.; Pulkin, A.; Wickenburg, S.; Ryu, H.; Ugeda, M. M.; Kastl, C.; Chen, C.; Hwang, C.; Schwartzberg, A.; Aloni, S.; Mo, S.-K.; Frank Ogletree, D.; Crommie, M. F.; Yazyev, O. V.; Louie, S. G.; Neaton, J. B.; Weber-Bargioni, A. Identifying Substitutional Oxygen as a Prolific Point Defect in Monolayer Transition Metal Dichalcogenides. *Nat Commun* **2019**, 10 (1), 3382.
- (5) Schuler, B.; Qiu, D. Y.; Refaely-Abramson, S.; Kastl, C.; Chen, C. T.; Barja, S.; Koch, R. J.; Ogletree, D. F.; Aloni, S.; Schwartzberg, A. M.; Neaton, J. B.; Louie, S. G.; Weber-Bargioni, A. Large Spin-Orbit Splitting of Deep In-Gap Defect States of Engineered Sulfur Vacancies in Monolayer WS₂. *Phys. Rev. Lett.* **2019**, 123 (7), 076801.